

## Nickel-Chitosan Hybrid as a Precursor for Nickel Oxide Nanoporous Particles for Organic Dyes Photodegradation

F. Farzaneh<sup>\*</sup>, Z. Asgharpour

*Department of Chemistry, Faculty of Sciences, Alzahra University, P.O. Box1993891176 Vanak, Tehran, Islamic Republic of Iran*

Received: 16 March 2014 / Revised: 10 June 2014 / Accepted: 28 June 2014

### Abstract

Hydrothermal synthesis of nickel-chitosan hybrid has been accomplished using  $\text{Ni}(\text{CH}_3\text{COO})_2 \cdot 4\text{H}_2\text{O}$ , chitosan and water as starting material, template and solvent respectively, followed by calcination at 800 and 900°C to provide nanoporous  $\text{NiO}_{800}$  and  $\text{NiO}_{900}$ . The solid products were characterized by X-ray diffraction (XRD), nitrogen adsorption-desorption, scanning electron microscopy (SEM) and Fourier transform infrared (FT-IR) techniques.  $\text{NiO}_{800}$  proved to be active for adsorption of Congo red with pseudo-second order kinetic model and adsorption isotherms, respectively fitted by Freundlich equation.  $\text{NiO}_{900}$  was also found to successfully catalyze the photodegradation of organic dye pollutants such as Congo red and methylene blue. The kinetic of photocatalytic behavior of  $\text{NiO}_{900}$  have proven to obey the first order and Langmuir–Hinshelwood model.

**Keywords:** Nanoparticles; Nickel Oxide; Photodegradation; Adsorption; Organic dyes.

### Introduction

The removal of toxic pollutants from industrial waste water reduce their environmental impact and health effects [1]. Whereas organic dyes are an important class of materials widely used in textile and many other industries, their hazardous effects in waste water have been a major concern. Several methods for removal of the dye contaminants from wastewater including adsorption [2], coagulation/flocculation [3], advanced oxidation processes [4], ozonation [5], membrane filtration [6] and biological treatments [7] have been developed and use. Amongst which, adsorption has been recognized as the most popular treatment process in aqueous solution with the advantages of high efficiency, simple operation, easy recovery and reuse of adsorbent. Several adsorbent

materials including clays [8], cellulose-based wastes [9], fly ash [10] and microorganisms [11] are examples in this regard. Since adsorption is a non-destructive method that simply transfers the dye from one phase/substance to another, often it is inadequate and/or inappropriate for removing large amounts of organic dyes from waste water streams. In contrast, advanced oxidation processes (AOP) have the capability of converting dye molecules into non-toxic compounds [12]. Among AOPs, heterogeneous photocatalytic oxidation has received considerable attention for destructive oxidation of dyes and textile effluents, since many aromatic compounds have proven to be degraded effectively to  $\text{CO}_2$ ,  $\text{H}_2\text{O}$  and small molecules [13, 14]. Catalysts such as inorganic-organic hybrids [15],  $\text{TiO}_2$  [1],  $\text{ZnO}$  [16],  $\text{ZnS}$  [17],

<sup>\*</sup> Corresponding author: Tel: +982188041344; Fax: +9821880441344; Email: faezeh\_farzaneh@yahoo.com, farzaneh@alzahra.ac.ir

CdS [18], and Fe<sub>2</sub>O<sub>3</sub> [19] have been reported for photodegradation. However, there are challenges for development and controlling parameters for new heterogeneous photocatalysis systems and deeper investigation on catalyst operation together with performance evaluation and other relevant aspects.

Although nanostructure NiO has many application in a wide range of area such as catalysis [20] electro chromic films [21], fuel cell electrodes [22], gas sensors [23], but there has been limited studies on heterogeneous catalysts and photocatalytic processes [24]. There are different methods reported for the synthesis of NiO nanoparticles such as hydrothermal or solvothermal synthesis [25-26], pulsed laser ablation [27], microemulsion [28], precipitation-calcination [29], sonochemical [30-31] and sol-gel methods [32]. Particularly significant is hydrothermal synthesis as a well-known method for the preparation of microporous crystals, complex oxides and inorganic-organic hybrid materials [33].

In this study, nickel-chitosan hybrid has been prepared hydrothermally using Ni(CH<sub>3</sub>COO)<sub>2</sub>·4H<sub>2</sub>O, chitosan and water as starting material, template and solvent respectively, followed by calcination at appropriate temperature in order to prepare nanoporous NiO. Congo red and methylene blue as cationic and anionic dyes served as model dyeing pollutant to evaluate the adsorption and photocatalytic degradation activity of the prepared catalysts.

## Materials and Methods

### Materials and Instruments details

All solvents and chemicals such as nickel acetate, chitosan, potassium hydroxide, ethanol 98%, acetic acid, Congo red and methylene blue were purchased from Merck Chemical Company and used without further purification.

Powder X-ray diffraction (XRD) data were recorded on XRD 3003 PTS Seifert with Cu K $\alpha$  radiation ( $\lambda=1.54\text{\AA}$ ). FTIR spectra were measured on KBr disks with a Bruker-Tensor 27 2002 spectrometer. Scanning electron micrograph (SEM) images were taken by XL-30 Phillips (1992). TGA thermal curve was studied by Perkin-Elmer Pyrif 1. Nitrogen adsorption was recorded at 77K by means of a Quanta Chrome Nova version 2.2 Analyzer and degradation progress was monitored by UV-Vis spectroscopy using a Unicam 8700 series spectrometer.

### Preparation of Catalysts

Nickel acetate solution (100 mL, 0.2 mol/L) was slowly added to the chitosan solution (1.6 gr, 100

mmol in 80 mL acetic acid 3% V/V). The mixture was heated in a 100 mL autoclave at 130 °C for 24 h. The resultant gel was washed with ethanol and dried. Calcination of the sample at 800 and 900 °C for 6 h afforded NiO<sub>800</sub> and NiO<sub>900</sub>, respectively.

### Photocatalytic evaluation

Congo red and methylene blue were used as dye pollutant sample in this study. NiO<sub>900</sub> (0.5 g) was added into the dye solution (50 ppm, 100 mL) while stirring. For methylene blue solution, pH was adjusted at 11 with NaOH (0.4 N). A 55W UV lamp was used as light source. The distance between the UV lamp and pyrex vessel containing catalyst and dye solution was fixed at 8 cm. Air was bubbled into the solution throughout the entire experiment to provide a constant source of dissolved oxygen. Prior to irradiation, the set up was kept in the dark for about 15 min in order to reach an adsorption/desorption equilibrium among the photocatalyst particles, dye and atmospheric oxygen molecules. The UV lamp was then turned on. During irradiation, the degraded dye was sampled in regular intervals and then centrifuged. The photocatalytic degradation was monitored by measuring the sample absorbance with a UV spectrophotometer. The degradation of dye was calculated using the following formula:

Degradation =  $(A_0 - A) / A_0$ , where  $A_0$  and  $A$  are the absorbance of the primal and remaining dye, respectively.

### Adsorption studies

Adsorption equilibrium experiments were carried out by adding the desired amount of NiO<sub>800</sub> as adsorbent to 100 mL of Congo red solution with known concentration at pH = 7 at ambient temperature. The mixture was vigorously stirred over 110 min as equilibrium time. The suspension was then centrifuged and the final concentration of dye solution was measured using an UV-Vis spectrophotometer at  $\lambda_{\text{max}} = 497$  nm. The equilibrium adsorbed Congo red concentration was calculated using the equation  $q_e = V(C_0 - C_e) / W$  in which  $C_0$ ,  $C_e$ ,  $V$  and  $W$  stand for the Congo red initial and equilibrium concentrations (mg/L), solution volume (L) and used adsorbent mass (g), respectively.

## Results and Discussion

### Catalysts characterization

The FTIR spectra of chitosan, Ni(II)/chitosan hybrid, calcined NiO<sub>800</sub> and NiO<sub>900</sub> are shown in Fig1.a-d, respectively. The broad peak centered at

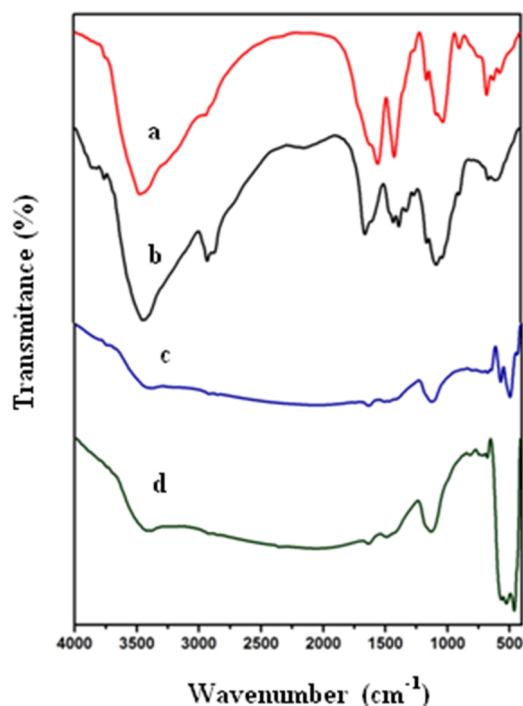


**Figure 1.** FTIR Spectra of (a) chitosan (b) as prepared Ni(II)/chitosan hybrid, (c) NiO nano spheres obtained after calcinations at 800 °C, for 6 h, (d) NiO nano spheres obtained after calcination at 900 °C, for 6 h.

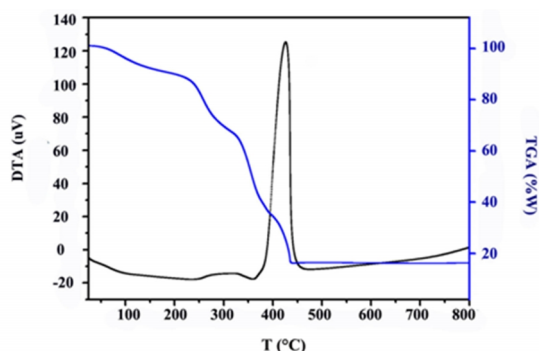


**Figure 2.** TGA and DTA curves of Ni-Chitosan hybrid.

$3450\text{ cm}^{-1}$  in all four spectra is due to the stretching vibrations of OH present in chitosan and adsorbed water. The vibration bands at the region 2948, 2869, 1623 and  $1153\text{ cm}^{-1}$  reveal the chitosan  $\text{CH}_2$ ,  $\text{NH}_2$  and C-O-C groups, respectively. The intensity of these peaks decrease after calcination to 800 °C due to the decomposition of chitosan (Fig.1.c, d). Whereas an increase in temperature to 800 °C decreases the vibration mode due to the chitosan decomposition, an increase and decrease in a peak intensity at  $1200\text{ cm}^{-1}$  is observed for the C-N or C-OH vibrations of

adsorbed species on NiO surface prior to and beyond 900 °C, respectively (Fig.1.d). Two new peaks were also found at  $490$  and  $445\text{ cm}^{-1}$  (Fig. 1d) due to the Ni-O stretching vibrations [34-36].

In order to reveal the changes occur during heat treatment of the prepared hybrid powder, the sample TGA and DTA were carried out within 30° to 900 °C in atmosphere. As seen in TGA curve (Fig. 2a), the major weight loss occur below 410 °C. It also reveal 5% weight loss in the temperature range of 50-120 °C due to the evaporation of adsorbed water. Observing an exothermic peak at 410 °C in DTA (Fig. 2b) might be due to the chitosan (template) decomposition and formation of NiO with 71% weight loss.

The SEM images of nanoparticles  $\text{NiO}_{800}$  and  $\text{NiO}_{900}$  with particle sizes of 25 and 35 nm are shown in Fig. 3a,b respectively.

The XRD patterns of the calcined Ni (II)/chitosan at 800° and 900 °C are shown in Fig. 4(a,b) respectively. As indicated, the XRD patterns of calcined NiO at 800° and 900 °C are similar. Whereas amorphous NiO phases were obtained after heating up to 200 °C, increasing the temperature to 800° and 900 °C afforded crystalline phases. The calcined samples at 800 ° and 900 °C exhibited the diffraction angle and characteristic peak intensities consistent with those of the standard JCPDS card no. (04-0835). The main diffraction peaks were observed at  $2\theta$   $37.13^\circ$ ,  $43.35^\circ$ ,  $63.11^\circ$ ,  $75.80^\circ$  and  $79.22^\circ$ .

All diffraction peaks can be indexed to the pure NiO crystalline phase (space group:  $\text{Fm}\bar{3}\text{m}$ ) and no peaks due to impurity were observed in the XRD pattern.

The textural characteristic of NiO nanospheres was investigated by the gas sorption measurement at 77 K. The nitrogen adsorption-desorption isotherms of the  $\text{NiO}_{800}$  and  $\text{NiO}_{900}$  are depicted in Fig.5 and the inset shows the Barrett-Joyner-Halenda (BJH) pore size distributions obtained from the adsorption branch. The specific surface area of  $\text{NiO}_{800}$  and  $\text{NiO}_{900}$  are  $6.8$  and  $3.7\text{ m}^2\text{g}^{-1}$ , respectively. Both NiO samples can be categorized as IUPAC type IV isotherms with  $\text{H}_3$  type hysteresis. The pore sizes of  $\text{NiO}_{800}$  and  $\text{NiO}_{900}$  are 3.45 nm and 3.36 nm, respectively. It is noticed that the pore size distribution curves of  $\text{NiO}_{800}$  and  $\text{NiO}_{900}$  show bimodal porosity. As such, it provides an efficient transport pathway for reactants of the  $\text{NiO}_{800}$  and  $\text{NiO}_{900}$  interiors, a beneficial catalytic property.

#### Photo-catalytic evaluations

The adsorption of cationic methylene blue and anionic Congo red dyes on the catalyst surface is important in photodegradation. Similarly, electric

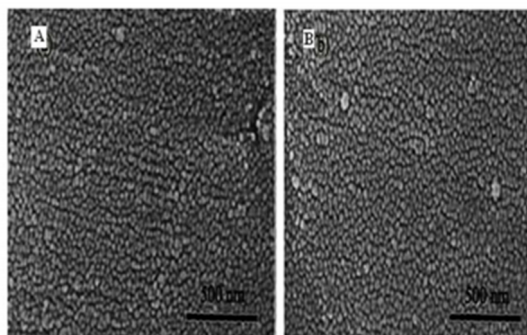


**Figure 3.** SEM images of NiO nanoparticles calcinated at (a) 800°C (b) 900°C for 6h.

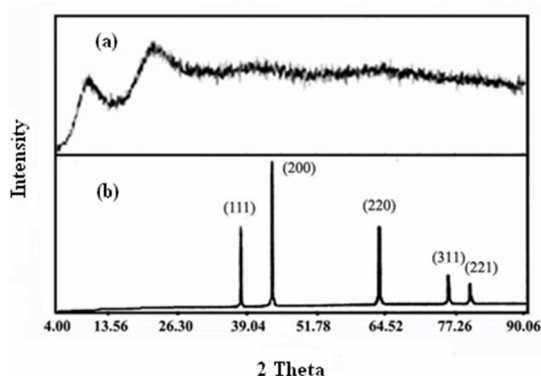


**Figure 4.** XRD patterns of (a) as-prepared Ni(II)/Chitosan hybrid (b) after calcination at 800 and 900°C.

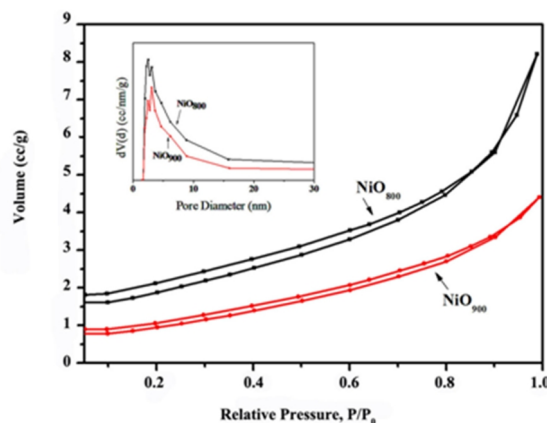


**Figure 5.** N<sub>2</sub> adsorption and desorption isotherms of NiO<sub>800</sub> and NiO<sub>900</sub>. Inset is the corresponding pore size distribution of NiO<sub>800</sub> and NiO<sub>900</sub>.

charge properties of both catalyst and substrate play an important role on adsorption process. Moreover, the nano NiO shows amphoteric behavior in aqueous media. The point of zero charge (pzc) of nano NiO, was found to be 10.5 [37]. Notably, nano NiO surface was found to be negatively charged and in protonated

form at pH higher than  $pH_{pzc}$  and lower pH values, respectively. For the adsorption of dye on NiO surface, photodegradation processes of methylene blue and Congo red were conducted at alkaline and natural pH using UV-Vis absorptions at wavelength of 664 and 497 nm, respectively.

The absorbance decrease after adding NiO nano particles and upon reaching equilibrium in dark for 15 min prior to irradiation onto the NiO surface due to the calculated 10 and 5% adsorption of Congo red and methylene blue, respectively. As observed in Fig. 6, under UV irradiation the intensity of the 497 nm and 664 nm absorption bands in the visible region due to the chromophores decreased rapidly and almost disappeared after 20 min and 90 min respectively.

The heterogeneous photocatalysis kinetic models have proven to obey the Langmuir–Hinshelwood (L–H) kinetic expression 1.

$$r = dC/dt = kKC / (1 + KC) \quad (1)$$

where  $r$ ,  $C$ ,  $t$ ,  $k$  and  $K$  are reactant oxidation rate (mg/l min), reactant concentration (mg/l), illumination time (s), reaction rate constant (mg/l min) and reactant adsorption coefficient (l/mg), respectively. If one works with low initial concentrations, the equation is simplified to an apparent first-order equation 2.

$$\ln(C_0/C) = kt \quad (2)$$

Where  $C_0$  and  $C$  are the dye concentrations at zero and  $t$  times, respectively. A plot of  $\ln C_0/C$  versus time then represents a straight line, the slope of which upon linear regression equals the apparent first-order rate constant  $k$ . As illustrated in Fig.6, obtaining linear plots of  $\ln (C_0/C)$  versus irradiation time for Congo red and methylene blue suggest that the photodegradation reactions follow the first order kinetics. The slopes of  $\ln (C_0/C)$  versus time plots in optimized conditions then give  $0.102 \text{ min}^{-1}$  and  $0.0269 \text{ min}^{-1}$  as the corresponding rate constants, respectively.

#### Adsorption studies

Adsorption equilibrium experiments were carried out by vigorous stirring of NiO<sub>800</sub> in desired amount as adsorbent and 100 ml of Congo red solution in known concentration at natural pH and ambient temperature within 110 min as equilibrium time. The suspension was then centrifuged and the final dye concentration was measured using an UV-Vis spectrophotometer at  $\lambda_{max} = 497 \text{ nm}$ . Congo red uptake at equilibrium adsorbed was calculated by means of  $q_e = V(C_0 - C_e) / W$  equation in which  $C_0$  and  $C_e$  (mg/L) stands for the

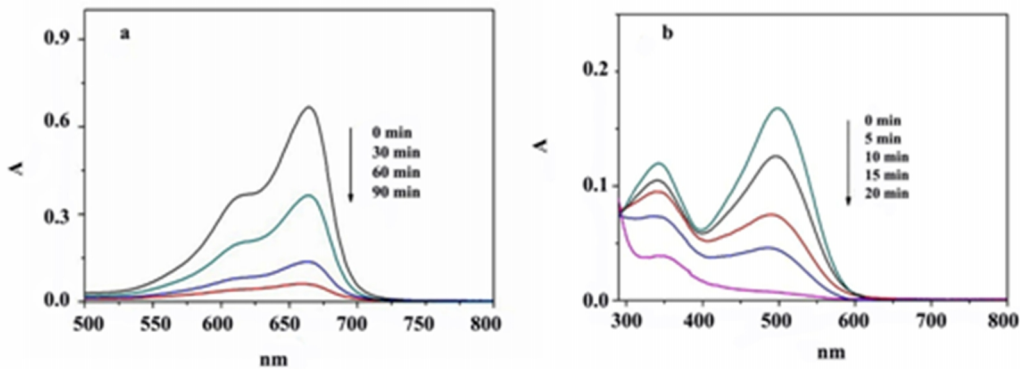


**Figure 6.** UV-Vis spectra changes of, Methylene blue(5ppm) (a) Congo red (5 ppm) (b) in aqueous NiO<sub>900</sub> dispersion under illumination at different times.

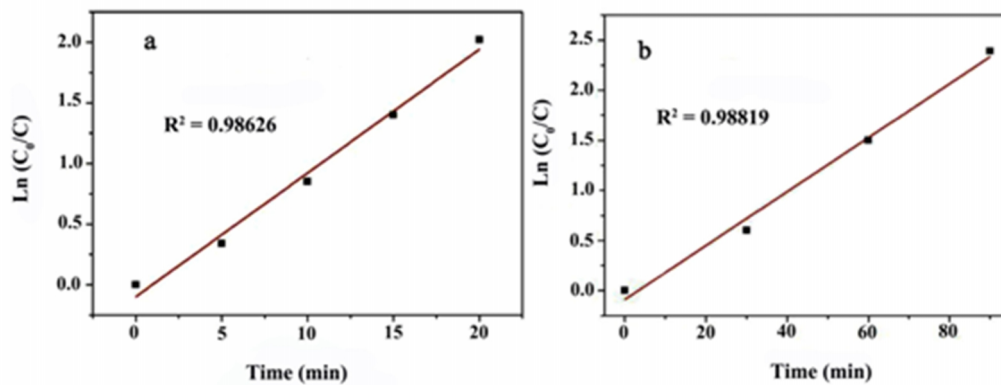


**Figure 7.** Plot of  $\ln(C_0/C)$  versus T for (a) Congo red and (b) Methylene blue.

Congo red concentrations at initial and equilibrium times respectively, V (L) as the solution volume and W (g) as the used adsorbent mass.

### Equilibrium isotherm modeling

To simulate the interaction between Congo red and NiO<sub>800</sub>, the equilibrium experimental data were analyzed using two commonly Freundlich and Langmuir isotherm models as are listed below:

Freundlich isotherm:

The adsorption equilibrium of the dye in solution and on the adsorbent surface using a multi-site adsorption isotherm for heterogeneous surfaces especially those involving organic compounds is described by equation 3 [38].

$$q_e = K_F C_e^{1/n} \quad (3)$$

It rearranges to linear equation 4 by taking the logarithm.

$$\log q_e = \log K_F + 1/n \log C_e \quad (4)$$

Where  $q_e$  (mg/g) and  $C_e$  (mg/L) represent the Congo red concentration adsorbed on NiO<sub>800</sub> and in solution at equilibrium, respectively and  $K_F$  and  $1/n$  stand for the Freundlich adsorption isotherm constants that can be calculated from intercept and slope of the linear plot between  $\log C_e$  and  $\log q_e$ .

Langmuir isotherm:

The Langmuir theory describes the monolayer coverage of adsorbent on a homogeneous adsorbent surface. The adsorption isotherm is based on the assumption that sorption takes place at specific homogeneous sites with constant adsorption energy. The adsorbed dyes were correlated by two parameters (equation 5).

$$q_e = q_m K_L C_e / (1 + K_L C_e) \quad (5)$$

Rearranging equation 5 gives equation 6.

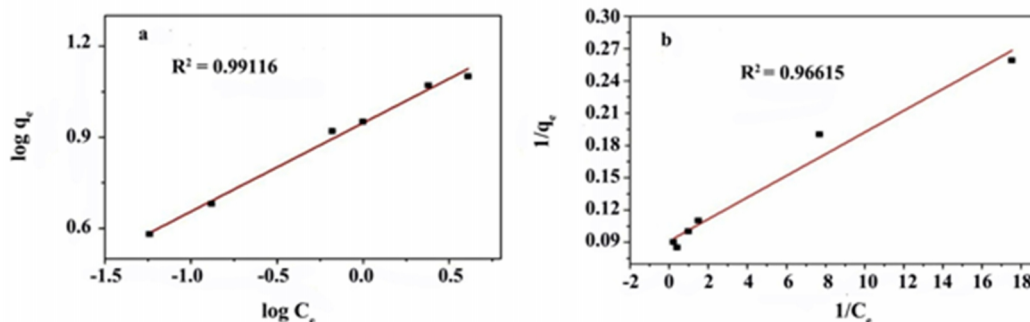


Figure 8. Adsorption isotherms for adsorption of Congo red on NiO<sub>800</sub> (a) Freundlich and (b) Langmuir.

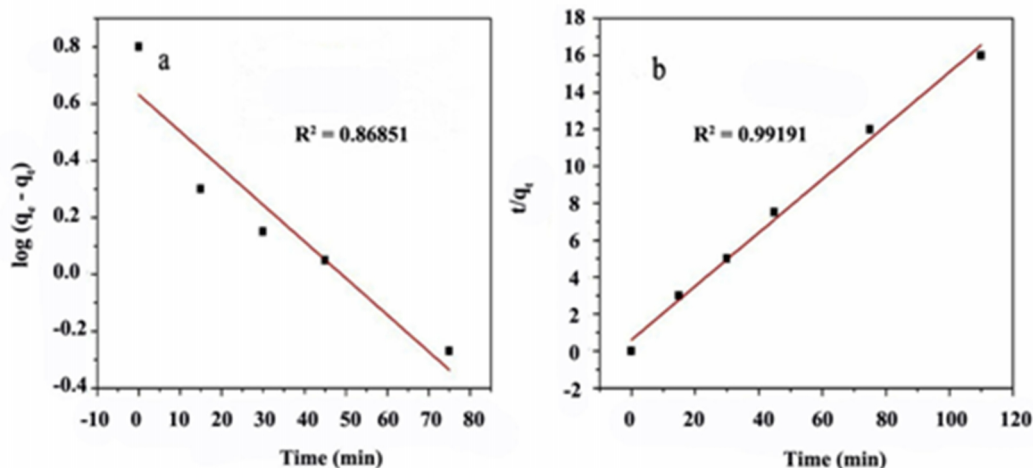


Figure 9. Adsorption kinetic for adsorption of Congo red on NiO<sub>800</sub> (a) Pseudo-first order and (b) Pseudo-second order.

$$1/q_e = 1/q_m + 1/K_L q_m 1/C_e \tag{6}$$

Where  $C_e$  (mg/L),  $q_e$  (mg/g) and  $q_m$  (mg/g) are the concentration and the amount of Congo red at equilibrium, adsorbed and the theoretical maximum adsorption capacity at equilibrium corresponding to monolayer coverage on NiO<sub>800</sub>, respectively.  $K_L$  (L/mg) is the Langmuir isotherm constant related to the energy of adsorption, respectively which can be determined from the linear plot of  $1/C_e$  versus  $1/q_e$ . The adsorption isotherms of Congo red on NiO<sub>800</sub> are shown in Fig.7.

The adsorption of Congo red on NiO<sub>800</sub> exhibits better fit to Freundlich equation by giving greater  $R^2$  value (Table 1). This adsorptive behavior indicates that there are various active sites on NiO<sub>800</sub>. As such, it can be concluded that adsorption takes place on a heterogeneous surface.

**Adsorption kinetic study**

In order to investigate the adsorption process of Congo red on the NiO<sub>800</sub>, pseudo-first order and pseudo second-order kinetics were experimented. Pseudo-first order equation 7 is widely used for the adsorption of an adsorbant from an aqueous solution [39].

$$dq_t/dt = k_1(q_e - q_t) \tag{7}$$

Where  $q_e$  and  $q_t$  (mg/g) are adsorbed dye at equilibrium and time  $t$ , respectively. By integration, it rearranges to equation 8.

$$\log(q_e - q_t) = \log q_e - k_1 t / 2.303 \tag{8}$$

The pseudo-first order rate constant  $k_1$  (min<sup>-1</sup>) was calculated as the slope of plot  $\log(q_e - q_t)$  against  $t$ . The pseudo second-order kinetic model (equation

**Table 1.** Isotherm data value of the fitted Freundlich and Langmuir model.

Langmuir	
$q_m$ (mg/g)	10.9565
$K_L$ (l/mg)	0.904
$R^2$	0.96615
Freundlich	
$K_F$ (mg/g (mg/l) <sup>-1/n</sup> )	8.852
$n$	3.427
$R^2$	0.9911

9) its integrated form (equation 10) were represented by Ho and McKay [40].

$$dq_t/dt = k_2(q_e - q_t)^2 \quad (9)$$

$$t/q_t = 1/k_2 q_e^2 + t/q_e \quad (10)$$

The  $q_e$  and  $k_2$  can be obtained by linear plot of  $t/q_t$  versus  $t$ .

The pseudo-first order and second order kinetics of Congo red adsorption on NiO<sub>800</sub> are shown in Fig. 8. The calculated kinetic parameters show that the mechanism follows Pseudo-second order model with extremely high linearity ( $R^2 = 0.99191$ ).

The best-fit to the pseudo-second order kinetics indicates that the adsorption mechanism depends on both adsorbed dye and adsorbent [41].

To the best of our knowledge, many catalysts have been used for adsorption and photodegradation of organic pollutants, but there are few reports using NiO nanoparticles as photodegradation catalyst. Among various methods for preparation of NiO nanoparticles, the hydrothermal method has more advantages such as simple process, easier to obtain high purity products and low cost. Hence, it is quite promising and easy to use for industrial applications.

In summary, The hydrothermal synthesis of Ni-chitosan hybrid and its use as precursor for the synthesis of NiO<sub>800</sub> and NiO<sub>900</sub> was described. It was found that NiO<sub>800</sub> is active for adsorption of Congo red and the kinetics as well as adsorption isotherms were fitted by pseudo-second order and Freundlich equation, respectively. Complete mineralization reactions of methylene blue and Congo red dyes can be effectively photo-catalyzed by NiO<sub>900</sub> nanoparticles under UV radiations. The photodegradation kinetic of both dyes with NiO<sub>900</sub> were proven to follow the first order.

## References

- Gupta V.K., Jain R., Mittal A., Saleh T.A., Nayak A., Agarwal S., and Sikarwar S. Photo-catalytic degradation of toxic dye amaranth on TiO<sub>2</sub>/UV in aqueous suspensions, *Mater. Sci. Eng. C*, **32**: 12-17 (2012).
- Crini G. and Badot P.M., Application of chitosan, a natural aminopoly-saccharide, for dye removal from aqueous solutions by adsorption processes using batch studies, *Prog. Polym. Sci.* **33**: 399-447(2008).
- Riera-Torres M., Gutiérrez-Bouzán C., and Crespi M., Combination of coagulation-flocculation and nanofiltration techniques for dye removal and water reuse in textile effluents, *Desalination*. **252**: 53-59 (2010).
- Banerjee P., DasGupta S., and De S., Removal of dye from aqueous solution using a combination of advanced oxidation process and nanofiltration. *J. Hazard. Mater.*, **140**: 95-103(2007).
- Konsowa A., Decolorization of wastewater containing direct dye by ozonation in a batch bubble column reactor, *Desalination*, **158**: 233-240 (2003).
- Kim T.H., Park C. and Kim S., Water recycling from desalination and purification process of reactive dye manufacturing industry by combined membrane filtration. *J. Clean. Prod.*, **13**: 779-786 (2005).
- Lodha B. and Chaudhari S., Optimization of Fenton-biological treatment scheme for the treatment of aqueous dye solutions. *J. Hazard. Mater.*, **148**: 459-466 (2007).
- Sethuraman V.V., Raymahashay B.C. Color removal by clays. Kinetic study of adsorption of cationic and anionic dyes. *Environ. Sci. Technol.* **9**: 1139-1140(1975).
- Annadurai G., Juang R.S., and Lee D.J. Use of cellulose-based wastes for adsorption of dyes from aqueous solutions. *J. Hazard. Mater.*, **92**: 263-274(2002).
- Li L., Wang S., and Zhu Z., Geopolymeric adsorbents from fly ash for dye removal from aqueous solution. *J. Colloid Interface Sci.* **300**: 52-59(2006).
- Chen K.C., Wu J.Y., Huang C.C., Liang Y.M., and Hwang S.C.J., Decolorization of azo dye using PVA-immobilized microorganisms, Silver nanoparticles on amidoxime fibers for photo-catalytic degradation of organic dyes in waste water. *J. Biotechnol.* **101**: 241-252 (2003).
- Wu Z.-C., Zhang Y., Tao T.-X., Zhang L., and Fong H., Silver nanoparticles on amidoxime fibers for photocatalytic degradation of organic dyes in waste water. *Appl. Surf. Sci.*, **257**:1092-1097(2010).
- Fox M.A., and Dulay M.T., Heterogeneous photocatalysis. *Chem. Rev.*, **93**: 341-357(1993).
- Matthews R.W., PHotooxidative degradation of coloured organics in water using supported catalysts, TiO<sub>2</sub> on sand. *Water Res.*, **25**: 1169-1176(1991).
- Jiao Y.Q., Qin C., Sun C.Y., Shao K.Z., Liu P.J., Huang P., Zhou K. and Su Z.M., Hydrothermal synthesis and structural characterization of a new inorganic-organic hybrid compound with photocatalytic activity based on Keggin-type polyanion and cadmium-1, 2, 4-triazolate units. *Inorg. Chem. Commun.*, **20**: 273-276 (2012).
- Wang Y., Li X., Lu G., Chen G., and Chen Y., Synthesis and photo-catalytic degradation property of nanostructured-ZnO with different morphology. *Mater. Lett.* **62** 2359-2362(2008).
- Li J., Xu Y., Liu Y., Wu D., and Sun Y., Synthesis of hydrophilic ZnS nanocrystals and their application in photocatalytic degradation of dye pollutants. *China Paarticuology*, **2** 266-269(2004).
- Li X., Hu C., Wang X., and Xi Y., PHotocatalytic activity

- of CdS nanoparticles synthesized by a facile composite molten salt method. *Appl. Surf. Sci.*, **258**: 4370-4376 (2012).
19. Cha H.G., Kim C.W., Kim Y.H., Jung M. H., Ji E.S., Das B.K., Kim J.C., and Kang Y.S., Preparation and characterization of  $\alpha$ -Fe<sub>2</sub>O<sub>3</sub> nanorod-thin film by metal-organic chemical vapor deposition, *Thin Solid Films*, **517**: 1853-1856 (2009).
  20. Berchmans S., Gomathi H., and Rao G.P., Electrooxidation of alcohols and sugars catalyzed on a nickel oxide modified glassy carbon electrode, *J. Electroanal. Chem.* **394**: 267-270 (1995).
  21. Kitao M., Izawa K., Urabe K., Komatsu T., Kuwano S., and Yamada S., Preparation and electrochromic properties of RF-sputtered NiO<sub>x</sub> films prepared in Ar/O<sub>2</sub>/H<sub>2</sub> atmosphere, Kinetics of the oxygen electrode reaction in molten Li<sup>+</sup> Na carbonate eutectic. *Jpn. J. Appl. Phys. Part 1*, **33**: 6656-6656 (1994).
  22. Tomczyk P., and Mordarski G. Kinetics of the oxygen electrode reaction in molten Li<sup>+</sup> Na carbonate eutectic. *J. Electroanal. Chem.*, **353**: 177-193(1993).
  23. Dirksen J.A., Duval K., and Ring T.A., NiO thin-film formaldehyde gas sensor. *Sensor. Actuat. B: Chem.* **80**: 106-115 (2001).
  24. Gondal M.A., Sayeed M.N., and Seddigi Z., Laser enhanced photo-catalytic removal of phenol from water using p-type NiO semiconductor catalyst. *J. Hazard. Mater.* **155**: 83-89 (2008).
  25. Wang X., Li L., Zhang Y., Wang S., Zhang Z., Fei L., and Qian Y., High-yield synthesis of NiO nanoplatelets and their excellent electrochemical performance. *Cryst. Growth Des.*, **6**: 2163-2165 (2006).
  26. Anadan K., Rajendran V., Morphological and size effects of NiO nanoparticles via solvothermal process. **14**: 43-47 (2011).
  27. Wang Y., and Qin Q.Z., A nanocrystalline NiO thin-film electrode prepared by pulsed laser ablation for Li-ion batteries. *J. Electrochem. Soc.*, **149**: A873 (2002).
  28. Han D., Yang H., Shen C., Zhou X., and Wang F., Synthesis and size control of NiO nanoparticles by water-in-oil microemulsion. *Powder Technol.*, **147**: 113-116 (2004).
  29. Xing W., Li F., Yan Z., and Lu G., Synthesis and electrochemical properties of mesoporous nickel oxide. *J. Power Sources*, **134**: 324-330 (2004).
  30. Aslania A., Oroojpoura V., and Fallahi M., Sonochemical synthesis, size controlling and gas sensing properties of NiO nanoparticles. *Appl. Surf. Sci.* **257**: 4056-4061(2011).
  31. Zhu W., Shui A., Xu L., Cheng X., Liu P. and Wang H., Template-free sonochemical synthesis of hierarchically porous NiO microsphere. *Ultrasound. Sonochem.* **21**: 1707-1713(2014).
  32. Yang Q, Sha J., Ma X., Synthesis of NiO nanowires by a sol-gel process, D. Yang, *Mater. Lett.*, **59** 1967-1970 (2005).
  33. Feng S., Xu R., New materials in hydrothermal synthesis. *Account. Chem. Res.*, **34**: 239-247 (2001).
  34. Enrique B.J. Spectroscopic investigation of the VO<sub>2</sub>+chitosan interaction, *Carbohydr. Polym.* **74**: 704-706 (2008).
  35. Braga T.P., Gomes E.C.C., Sousa A.F.d., Carreño N.L.V., Longhinotti E., Valentini A., Synthesis of hybrid mesoporous spheres using the chitosan as template. *J. Non-Cryst. Solids*, **355**: 860-866 (2009).
  36. Li Q., Kumar V., Li Y., Zhang H., Marks T.J. and Chang R.P.H., Fabrication of ZnO nanorods and nanotubes in aqueous solutions, *Chem. Mater.*, **17**: 1001-1006 (2005).
  37. Lewis J.A., Colloidal processing of ceramics. *J. Am. Ceram. Soc.*, **83**: 2341-2359 (2000).
  38. Gil A., Assis F.C.C., Albeniz S., and Korili S.A., Removal of dyes from wastewaters by adsorption on pillared clays. *Chem. Eng. J.*, **168**: 1032-1040 (2011).
  39. Vimonses V., Lei S., Jin B., Chow C.W.K., and Saint C., Kinetic study and equilibrium isotherm analysis of Congo red adsorption by clay materials. *Chem. Eng. J.*, **148**: 354-364 (2009).
  40. Ho Y. and McKay G., Sorption of dye from aqueous solution by peat, *Chem. Eng. J.* **70**: 115-124 (1998).
  41. Pavan F.A., Dias S.L.P., Lima E.C., and Benvenuti E.V., Removal of Congo red from aqueous solution by anilinepropylsilica xerogel. *Dyes & Pigments*, **76**: 64- 69 (2008).